TU Delft

Delft University of Technology

Consistent Regularization of Induced Coulomb Stresses in Displaced Faults

Jansen, J.D.

DOI
10.4233/uuid:98223aec-2a6a-4ad3-b3e7-a422e9dadfdd

Publication date
2023

Document Version
Final published version

Citation (APA)
Jansen, J. D. (2023). *Consistent Regularization of Induced Coulomb Stresses in Displaced Faults*. Delft University of Technology. https://doi.org/10.4233/uuid:98223aec-2a6a-4ad3-b3e7-a422e9dadfdd

Important note
To cite this publication, please use the final published version (if applicable).
Please check the document version above.

Copyright
Other than for strictly personal use, it is not permitted to download, forward or distribute the text or part of it, without the consent of the author(s) and/or copyright holder(s), unless the work is under an open content license such as Creative Commons.

Takedown policy
Please contact us and provide details if you believe this document breaches copyrights.
We will remove access to the work immediately and investigate your claim.

This work is downloaded from Delft University of Technology.
For technical reasons the number of authors shown on this cover page is limited to a maximum of 10.

Consistent Regularization of Induced Coulomb Stresses in Displaced Faults

Jan Dirk Jansen,
Dept. of Geoscience and Engineering
Delft University of Technology, The Netherlands
j.d.jansen@tudelft.nl

23 May 2023

Abstract

This note provides unregularized and regularized closed-form analytical expressions for the depletion-induced or injection-induced pre-slip Coulomb stresses in two-dimensional displaced dip-slip faults. The regularization serves to remove logarithmic singularities and jump-discontinuities in the unregularized formulation. The expressions are identical to those in Appendices A and B of Jansen & Meulenbroek (2022): *Netherlands Journal of Geosciences* **101** e13, except for the correction of a small error in the regularized formulation. In numerical examples the difference of the correction is hardly noticeable, but it ensures that the corrected formulation is internally consistent in the sense that integrals of stresses and pressure along a fault are identical for the unregularized and regularized expressions.

1 Introduction

The note is concerned with the computation of poroelastic pre-slip Coulomb stresses caused by injection or production of fluids into/from deep subsurface reservoirs. In particular it considers stress patterns that occur when these reservoirs contain displaced faults, i.e. faults with non-zero offset. The particular effect of fault offset on pre-slip Coulomb stresses and its consequences for induced fault slip seem to have been first adressed in relation to the depletion of hydrocarbon reservoirs, and early numerical studies into this aspect were made by Roest & Kuilman (1994), Roest & Mulders (2000) and Mulders (2003). More recent numerical studies were performed by Van den Bogert (2015, 2018), Buijze et al. (2017, 2019) and Van Wees et al. (2017, 2019) who all demonstrated the development of two shear stress peaks, resulting in two slip patches that grow with increasing depletion and may eventually merge. A detailed semi-analytical treatment of this effect was reported by Jansen & Meulenbroek (2022) who considered a two-dimensional plane-strain model of a reservoir, infinitely wide and of height $h = a + b$, intersected by a displaced non-sealing zero-width normal fault with throw $t_f = b - a$ and dip angle θ; see Figure 1.

From the studies listed above that addressed the effect of fault offset in detail it follows that depletion typically results in two zones of positive Coulomb stresses that may develop into slip patches. These two zones are located around the 'internal' reservoir-fault corners at $y = \pm a$; see Figure 2 which displays results for an example with parameter values given in Jansen & Meulenbroek (2022). Depending on the friction characteristics

of the fault, continuing depletion may result in a gradual aseismic growth of the two slip patches possibly leading to merging. Even further depletion may then lead to an unstable situation resulting in a seismic event. In another scenario, which seems to be more frequently occuring, one of the slip patches (or occasionally both) becomes unstable and generates an event before merging occcurs (Van den Bogert 2015, 2018, Buijze et al. 2017, 2019, Jansen & Meulenbroek 2022).

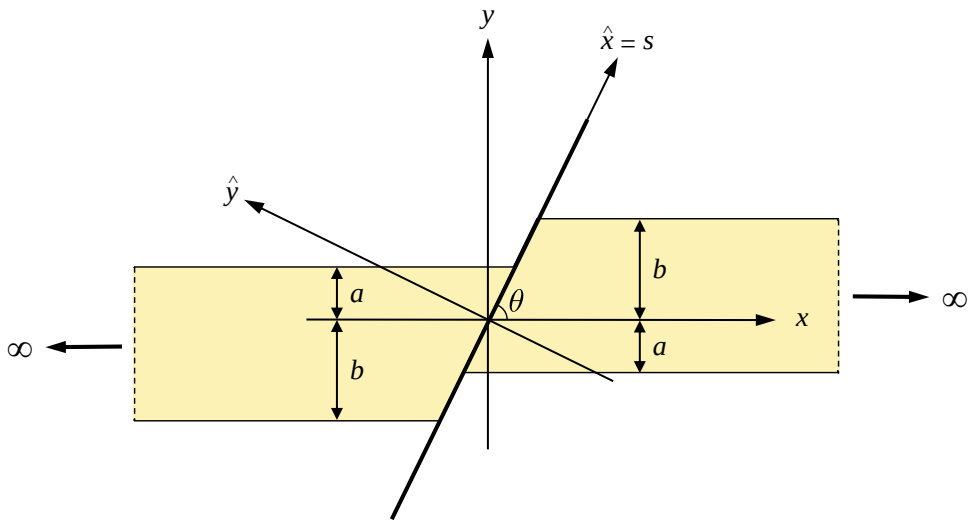

Figure 1: Infinitely wide reservoir with a displaced normal fault (Jansen & Meulenbroek 2022).

The presence of sharp 'internal' and 'external' reservoir-fault corners in the reservoir model displayed in Figure 1 results in positive-valued peaks in the pre-slip Coulomb stress at $y = \pm a$ and negative-valued peaks at $y = \pm b$, see Figure 2, which are, mathematically, of infinite magnitude. In reality, physical effects such as more rounded corners, a finite fault width and pore pressure diffusion between the reservoir and the surrounding rock will somewhat smoothen the stress profile. Jansen & Meulenbroek (2022) provided two versions of closed-form analytical expressions for induced pre-slip Coulomb stresses: one that results in four infinite stress peaks, and a second, regularized, version that describes more rounded peaks. This note serves to highlight the regularized version while correcting a minor error. Figures 1 and 2, and the material in Sections 2 and 3 of this note have been taken near-verbatim from Jansen & Meulenbroek (2022) except for the last paragraph of Section 2, equations (14) to (16) and Figure 3 with the corresponding text.

Irrespective of the use of regularization, relatively sharp peaks in the pre-slip Coulomb stress profile remain a typical characteristic of displaced faults that experience induced stresses. A second typical characteristic concerns the distinction in shape between injection and production: whereas depletion produces positive stress peaks at the internal corners and negative peaks at the external corners, injection results in positive peaks at the external corners and negative peaks at the internal ones (Jansen et al. 2019). Also, for increasing depletion the 'internal patches' will grow further inward with the negative stress peaks at the external corners blocking progression of the slip towards the overburden or underburden. Opposedly, during injection the external patches will grow outward, into the overburden and underburden, while also the increased reservoir pressure is more likely to propagate outward through the fault causing a further tendency of outward slip propagation.

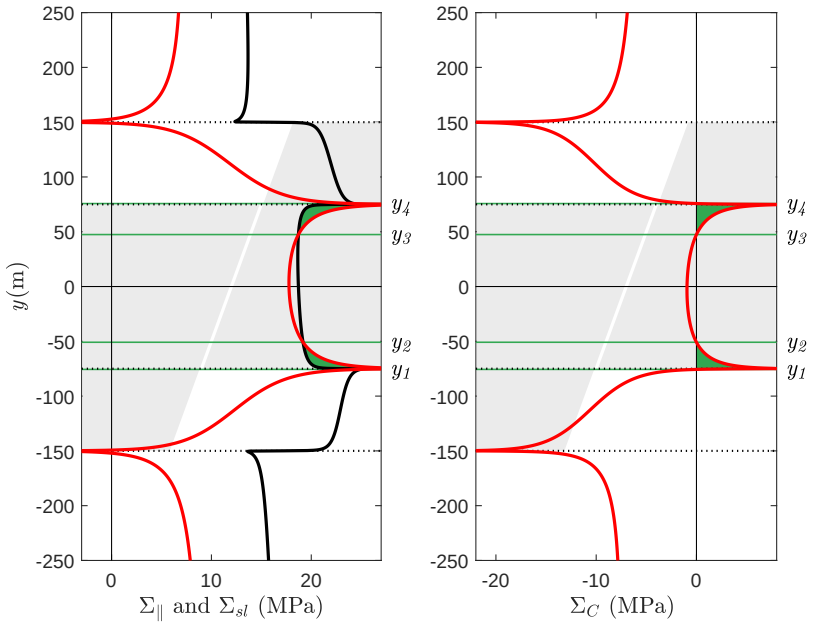

Figure 2: Shear stresses, slip threshold and pre-slip Coulomb stresses (Jansen & Meulenbroek 2022). Left: red lines represent the combined depletion-induced shear stresses $\Sigma_{||}$ and black lines the slip threshold Σ_{sl} as a function of vertical position y. Right: red lines represent the pre-slip Coulomb stresses $\Sigma_C = \Sigma_{||} - \Sigma_{sl}$. In both the left and right figures the green areas indicate those regions where the shear stresses exceed the slip threshold and, accordingly, the green horizontal lines at $y = -76$, -51, 47 and 76 m correspond to the intersections between shear stresses and slip threshold, i.e. the zeros of the pre-slip Coulomb stresses. The light gray areas depict the vertical positions of the foot wall and the hanging wall.

2 Initial and Incremental Stresses

We assume the presence of an initial regional stress pattern with principal stresses σ^0_{yy} (vertical) and

$$\begin{aligned} \sigma^0_{xx} &= \sigma'^0_{xx} - \alpha p^0 \\ &= K^0 \sigma'^0_{yy} - \alpha p^0 \\ &= K^0(\sigma^0_{yy} + \alpha p^0) - \alpha p^0, \end{aligned} \tag{1}$$

(horizontal), where α is Biot's coefficient, p^0 is the initial pore pressure (a superscript '0' means 'initial'), K^0 is the initial effective stress ratio, and where a primed stress variable σ' represents an 'effective stress'. We employ a sign convention where positive strains and stresses imply extension and tension, and where pore pressures are positive. The resulting initial normal and shear stresses acting on the fault follow from a coordinate rotation as

$$\sigma^0_{\perp} = \quad \sigma^0_{\tilde{y}\tilde{y}} = \sigma^0_{xx} \sin^2\theta + \sigma^0_{yy} \cos^2\theta, \tag{2}$$

$$\sigma^0_{||} = -\sigma^0_{\tilde{x}\tilde{y}} = (\sigma^0_{xx} - \sigma^0_{yy}) \sin\theta \cos\theta, \tag{3}$$

where $\tilde{x}$ and $\tilde{y}$ are rotated coordinates, and where θ is the dip angle of the fault; see Figure 1. A positive-valued shear stress $\sigma_{||}$ corresponds to a normal faulting regime, i.e. a situation where the hanging wall (to the left of the fault in Figure 1) has a tendency

to slide down from the foot wall (to the right of the fault). The initial effective normal stress acting at the fault follows as

$$\sigma'^{0}_{\perp} = \sigma^{0}_{\perp} + \beta p^{0}, \tag{4}$$

where β is an effective stress coefficient which is not necessarily identical to α and is often taken as unity Scholz (2019), Fjaer et al. (2021).

An increase or decrease in pore pressure in the reservoir will result in incremental normal and shear stresses in the reservoir and its surroundings. We restrict the analysis to the case of a quasi steady state, i.e. a spatially homogeneous incremental pore pressure $p(t)$ that is a slow function of time t. Closed-form analytical expressions for the corresponding incremental normal and shear stresses in the fault were obtained by Jansen et al. (2019) with the aid of inclusion theory and can be expressed as

$$\sigma_{\perp} = \left(-\sigma_{xy} \sin\theta \cos\theta + \sigma_{xx} \sin^2\theta\right), \tag{5}$$

$$\sigma_{\parallel} = \quad \left(\sigma_{xy} \sin^2\theta + \sigma_{xx} \sin\theta \cos\theta\right), \tag{6}$$

where $\sigma_{xx} = \sigma_{\tilde{y}\tilde{y}}$ and $\sigma_{xy} = -\sigma_{\tilde{x}\tilde{y}}$ are normal and shear stresses for a vertical fault, i.e. for a dip angle $\theta = \frac{\pi}{2}$. For an infinitely wide reservoir, they are defined as (see also Appendix A in Jansen & Meulenbroek (2022))

$$\sigma_{xx} = \begin{cases} 0 & \text{if} \quad y \leqslant -b \ \text{ or } \ b \leqslant y \\ -\pi C & \text{if} \quad -b < y \leqslant -a \ \text{ or } \ a \leqslant y < b \\ -2\pi C & \text{if} \quad -a < y < a \end{cases}, \tag{7}$$

and

$$\sigma_{xy} = \frac{C}{2} \ln \frac{(y-a)^2 (y+a)^2}{(y-b)^2 (y+b)^2}, \tag{8}$$

where $C(p(t))$ is a pressure-dependent scaling parameter, with SI units Newton per meter squared, defined as

$$C = \frac{(1-2\nu)\alpha p(t)}{2\pi(1-\nu)}, \tag{9}$$

with ν representing Poisson's ratio. For dipping as well as vertical faults the incremental effective normal stress is given by

$$\sigma'_{\perp} = \sigma_{\perp} + \begin{cases} 0 & \text{if} \quad y \leqslant -b \ \text{ or } \ b \leqslant y \\ \beta p & \text{if} \quad -b < y < b \end{cases}. \tag{10}$$

In the derivation of equation (10) it was assumed that only those parts of the fault that are in direct contact with the reservoir experience incremental reservoir pressure, i.e. that the relevant fault segment is given by $-b < y < b$. If a larger part of the fault is exposed to incremental pressure, the domain where βp is added should be extended accordingly.

Somewhat more elaborate closed-form expressions for a finite-width reservoir, derived with inclusion theory, are given in the paper by Jansen et al. (2019) and the accompanying Supporting Information. These can also be used to obtain the stresses in case of a fully sealing fault with different reservoir pressures to the left and the right of the fault. Moreover, if the width of the reservoir section to either side of the fault is taken as zero, these expressions describe the stresses in a bounding fault, or a sealing fault with zero depletion at one of the sides. Similar expression were published concurrently by Lehner (2019) and later by Wu et al. (2021). In case of a non-homogenous pressure field, inclusion theory can still be applied to obtain the fault stresses but the resulting integrals have

to be solved numerically, an approach that has been followed early-on by Segall (1985), and later by Van Wees et al. (2019) (who used 3D point-based expressions from Okada (1992) for the subdomains in the numerical quadrature), Smith et al. (2022) (who used 3D volume-based expressions from Kuvshinov (2008) which, unlike point-based expressions, don't suffer from near-fault anomalies), and Cornelissen & Jansen (2023) (who used the 2D expressions of Jansen et al. (2019) which are also volume based).

3 Regularized Expressions

Equations (5) and (6) for the incremental stresses contain logarithmic singularities and jump discontinuities at $y = \pm a$ and $y = \pm b$. A regularized form of the incremental stresses removes the singularities and discontinuities; see Appendix B in Jansen & Meulenbroek (2022). We quote the following expressions from that appendix:

$$\sigma^r_{xx} = -C\left\{\arctan 2\left[(a+b)\eta, \eta^2 + (y-b)(y+a)\right] + \arctan 2\left[(a+b)\eta, \eta^2 + (y-a)(y+b)\right]\right\}, \tag{11}$$

$$\sigma^r_{xy} = \frac{C}{2}\ln\frac{\left[\eta^2 + (y-a)^2\right]\left[\eta^2 + (y+a)^2\right]}{\left[\eta^2 + (y-b)^2\right]\left[\eta^2 + (y+b)^2\right]}, \tag{12}$$

where the 'arctan2' operation is defined for arguments (y, x) in the interval $[-\pi, \pi]$ according to

$$\arctan 2(y,x) = \begin{cases} \mathrm{sgn(y)} \cdot \arctan\left(\left|\frac{\mathrm{y}}{\mathrm{x}}\right|\right) & x > 0 \\ \mathrm{sgn(y)} \cdot \frac{\pi}{2} & x = 0, y \neq 0 \\ \text{undefined} & x = 0, y = 0 \\ \mathrm{sgn(y)} \cdot \left[\pi - \arctan\left(\left|\frac{\mathrm{y}}{\mathrm{x}}\right|\right)\right] & x < 0 \end{cases}. \tag{13}$$

Equations (11) and (12) can be used instead of equations (7) and (8) to which they can be shown to revert for $\eta = 0$. The corresponding regularized version of the second line in equation (10) for the effective normal stresses is given by

$$\sigma'^r_\perp = \sigma_\perp + \beta p^r = \sigma_\perp + \beta\frac{p}{\pi}\arctan 2\left[2b\eta, \eta^2 + (y-b)(y+b)\right]. \tag{14}$$

4 Consistency

Equation (14) contains a small correction of the original expression for $\sigma'^r_\perp$ in Jansen & Meulenbroek (2022): the first term inside the square brackets was originally taken as $(a+b)\eta$ whereas here we use $2b\eta$. In numerical examples the difference is hardly noticeable, but the current formulation is internally consistent, as demonstrated in the next paragraph, whereas the original formulation wasn't.

Both the unregularized and the regularized expressions can be integrated analytically and it can be shown that they result in exactly the same values:

$$\int_{-\infty}^{\infty}\sigma_{xx}(y)\,dy = \int_{-\infty}^{\infty}\sigma^r_{xx}(y)\,dy = -2\pi C(a+b), \tag{15}$$

$$\int_{-\infty}^{\infty}\sigma_{xy}(y)\,dy = \int_{-\infty}^{\infty}\sigma^r_{xy}(y)\,dy = 0, \tag{16}$$

$$\int_{-\infty}^{\infty}p(y)\,dy = \int_{-\infty}^{\infty}p^r(y)\,dy = 2bp. \tag{17}$$

This consistency implies that the regularization has only a local effect that does not disturb the global stress distribution in the fault. Also differentiation of the regularized expressions can be done analytically and the result for values around one of the infinite peaks in the pre-slip Coulomb stress has been displayed in Figure 3 (right). The corresponding maximum of the pre-slip Coulomb stress, depicted in Figure 3 (left), displays a small shift in location, of the same order of magnitude as the value of the regularization parameter η. A similar small shift is observed in the location of the pre-slip Coulomb stress zeros.

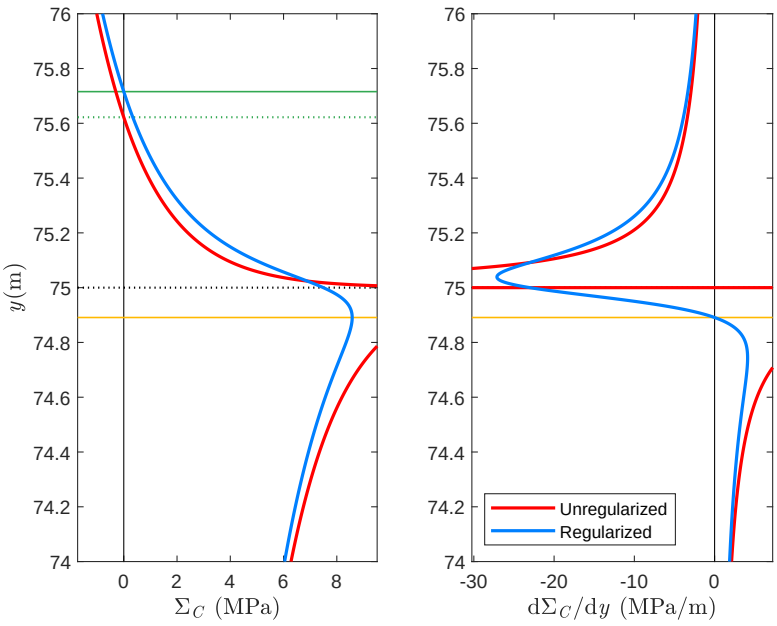

Figure 3: Pre-slip Coulomb stress Σ_C (left) and its spatial derivative $\frac{d\Sigma_C}{dy}$ (right) with and without regularization, in the neighbourhood the singularity at $y = a = 75.0$ m (dotted black line) which coincides with one of the four infinite-magnitude peaks of the unregularized version of Σ_C. The orange horizontal line at $y = 74.9$ m corresponds to the local zero of the regularized version of $\frac{d\Sigma_C}{dy}$ and therefore to the (finite) local maximum of the regularized version of Σ_C. The figure has been produced with parameter values for the example in Jansen & Meulenbroek (2022). The value of the regularization parameter is $\eta = 0.10$ m. As a result of the regularization the location of the maximum value of Σ_C has shifted over approximately the same distance. The same holds for the shift in location of the pre-slip Coulomb stress zeros; see the solid (regularized) and dotted (unregularized) green lines in the left plot.

5 Finite-Width Reservoir

The unregularized and regularized expressions in this note are valid for an infinitely wide reservoir. Detailed unregularized expressions for a finite-width reservoir are given in Jansen et al. (2019). We did not derive the corresponding regularized expressions, but in a numerical implementation the finite-width result can simply be obtained as:

$$\sigma_{xx}^{rf} = \sigma_{xx}^{f} + (\sigma_{xx}^{r} - \sigma_{xx}) \tag{18}$$

$$\sigma_{xy}^{rf} = \sigma_{xy}^{f} + (\sigma_{xy}^{r} + \sigma_{xy}), \tag{19}$$

where superscripts f and rf refer to *finite* and *regularized finite* respectively.

References

Buijze, A., Van den Bogert, P., Wassing, B. & Orlic, B. (2019), 'Nucleation and arrest of dynamic rupture induced by reservoir depletion', *Journal of Geophysical Research: Solid Earth* **124**, 3620–3645.
URL: *https://doi.org/10.1029/2018JB016941*

Buijze, A., Van den Bogert, P., Wassing, B., Orlic, B. & Ten Veen, J. (2017), 'Fault reactivation mechanisms and dynamic rupture modelling of production-induced seismic events in a Rotliegend gas reservoir', *Netherlands Journal of Geosciences* **96**, S131–S148.
URL: *https://doi.org/10.1017/njg.2017.27*

Cornelissen, P. & Jansen, J. (2023), 'Steady-state flow through a subsurface reservoir with a displaced fault and its poro-elastic effects on fault stresses', *Submitted* .

Fjaer, E., Holt, R., Horsrud, P., Raaen, A. & Risnes, R. (2021), *Petroleum Related Rock Mechanics,* 3^{rd} *ed.*, Elsevier.

Jansen, J. & Meulenbroek, B. (2022), 'Induced aseismic slip and the onset of seismicity in displaced faults', *Netherlands Journal of Geosciences* **101**(e13).
URL: *https://doi.org/10.1017/njg.2022.9*

Jansen, J., Singhal, P. & Vossepoel, F. (2019), 'Insights from closed-form expressions for injection- and production-induced stresses in displaced faults', *Journal of Geophysical Research: Solid Earth* **124**, 7193–7212.
URL: *https://doi.org/10.1029/2019JB017932*

Kuvshinov, B. N. (2008), 'Elastic and piezoelectric fields due to polyhedral inclusions', *International Journal of Solids and Structures* **45**(5), 1352–1384.
URL: *https://doi.org/10.1016/j.ijsolstr.2007.09.024*

Lehner, F. (2019), An analysis of depletion-induced fault stressing - new closed-form analytical solutions, Technical report, Nederlandse Aardolie Maatschappij.
URL: *http://www.nam.nl/feiten-en-cijfers/onderzoeksrapporten.html*

Mulders, F. (2003), Modelling of Stress Development and Fault Slip in and Around a Producing Gas Reservoir, PhD thesis, Delft University of Technology.
URL: *http://resolver.tudelft.nl/uuid:be742135-10d7-4d69-bdee-f808b5926065*

Okada, Y. (1992), 'Internal deformation due to shear and tensile faults in a half space', *Bulletin of the Seismological Society of America* **82**, 1018–1040.

Roest, J. & Kuilman, W. (1994), Geomechanical analysis of small earthquakes at the Eleveld gas reservoir, *in* 'SPE-ISRM Rock Mechanics in Petroleum Engineering Conference'. Paper SPE 28097. 29-31 Aug., Delft, The Netherlands.
URL: *https://doi.org/10.2118/28097-MS*

Roest, J. & Mulders, F. (2000), Overview modelling gas production-induced seismicity mechanisms, *in* 'Eurock 2000 Symposium'. 27–31 March, Aachen, Germany.
URL: *http://resolver.tudelft.nl/uuid:6913b331-83f4-499a-822a-6d2af5091580*

Scholz, C. (2019), *The Mechanics of Earthquakes and Faulting,* 3^{rd} *ed.*, Cambridge.

Segall, P. (1985), 'Stress and subsidence resulting from subsurface fluid withdrawal in the epicentral region of the 1983 Coalinga earthquake', *Journal of Geophysical Research* **90**, 6801–6816.
URL: *https://doi.org/10.1029/JB090iB08p06801*

Smith, J. D., Heimisson, E. R., Bourne, S. J. & Avouac, J.-P. (2022), 'Stress-based forecasting of induced seismicity with instantaneous earthquake failure functions: Applications to the Groningen gas reservoir', *Earth and Planetary Science Letters* **594**, 117697.

Van den Bogert, P. (2015), 'Impact of various modelling options on the onset of fault slip and fault slip response using 2-dimensional finite-element modelling'.
URL: *https://www.nam.nl/feiten-en-cijfers/onderzoeksrapporten.html*

Van den Bogert, P. (2018), 'Depletion-induced fault slip and seismic rupture: 2D geomechanical models for the Groningen field, the Netherlands'.
URL: *https://www.nam.nl/feiten-en-cijfers/onderzoeksrapporten.html*

Van Wees, J., Fokker, P., Van Thienen-Visser, K., Wassing, B., Osinga, S., Orlic, B., Ghouri, S., Buijze, L. & Pluymaekers, M. (2017), 'Geomechanical models for induced seismicity in the Netherlands: inferences from simplified analytical, finite element and rupture model approaches', *Netherlands Journal of Geosciences* **96**, S183–S202.
URL: *https://doi.org/10.1017/njg.2017.38*

Van Wees, J., Pluymaekers, M., Osinga, S., Fokker, P., Van Thienen-Visser, K., Orlic, B., Wassing, B., Hegen, D. & Candela, T. (2019), '3-d mechanical analysis of complex reservoirs: a novel mesh-free approach', *Geophysical Journal International* **219**, 1118–1130.
URL: *https://doi.org/10.1093/gji/ggz352*

Wu, H., Vilarrasa, V., De Simone, S., Saaltink, M. & Parisio, F. (2021), 'Analytical solution to assess the induced seismicity potential of faults in pressurized and depleted reservoirs', *Journal of Geophysical Research: Solid Earth* **126**, e2020JB020436.
URL: *https://doi.org/10.1029/2020JB020436*